Chapter 18

A Nonlinear Aeroelastic Model for the Study of Flapping Wing Flight

Rambod F. Larijani* and James D. DeLaurier†
University of Toronto, Downsview, Ontario, Canada

Nomenclature

A	=	element cross-sectional area
AR	=	aspect ratio
a	=	mass-proportional damping constant
b	=	stiffness-proportional damping constant
C_d	=	drag coefficient
C_{df}	=	skin-friction drag coefficient
C_{mac}	=	airfoil moment coefficient about its aerodynamic center
C_n	=	normal force coefficient
c	=	wing segment chord length
D_c	=	drag due to camber
D_f	=	friction drag
E	=	modulus of elasticity
F_y	=	total chordwise force
$F'(k)$, $G'(k)$	=	terms for modified Theodorsen function
G	=	shear modulus of elasticity
g_r	=	acceleration due to gravity
h	=	total plunging displacement
$\tilde{h}$	=	elastic component of plunging displacement
h_0	=	imposed displacement
I	=	moment of inertia
J	=	polar moment of inertia
k	=	reduced frequency based on $\frac{1}{2}c$
L	=	total lift
M	=	total twisting moment acting on a wing segment

*Ph.D. Student, Institute for Aerospace Studies.
†Professor, Institute for Aerospace Studies. Associate Fellow AIAA.

m = distributed moment per unit length
$\overline{m}$ = mass per unit length
N = total normal force acting on a wing segment
n = distributed normal force per unit length
P_1, P_2 = element boundary conditions for torsion
p = contact pressure
$Q_1, \ldots, Q_4$ = element boundary conditions for bending
R = total thrust
T_s = leading edge suction force
U = freestream velocity
V = relative velocity at $\frac{1}{4}$-chord location
V_y = relative velocity tangential to a wing segment
v_r = relative velocity of upper vs lower surface of the wing
x = distance from flapping axis to middle of segment
y = distance from the leading edge

Greek

α = relative angle of attack at $\frac{3}{4}$-chord point due to wing segment motion
α' = the flow's relative angle of attack at $\frac{3}{4}$-chord point
α_0 = wing segment's angle of zero-lift line
α_{stall} = segment stall angle
Γ_0 = magnitude of flapping dihedral angle
Δx = length of an element
$\Delta\bar{h}$ = nonflapping plunging displacement
$\Delta\bar{\theta}$ = nonflapping elastic twist
η_s = leading-edge suction efficiency
θ = total segment twist angle with respect to U
$\tilde{\theta}$ = elastic twist angle
$\bar{\theta}_a$ = angle of flapping axis with respect to U
$\bar{\theta}_{\text{wash}}$ = built-in pretwist
ρ = atmospheric density
ζ = decay constant
ψ = transverse twist angle (along local y axis)
ω = flapping frequency

Subscripts

a = apparent mass
ac = aerodynamic center
aero = aerodynamic
ave = average
c = circulatory
cf = crossflow
cs = center section
con = contact
damp = damping
dsr = shear rate dependent damping

ea = elastic axis
ef = effective
f = friction
fr = fabric and rib
inertia = inertial
rs = rigid section
s = spar
sep = separated flow
sr = super rib
st = static
te = trailing edge

Superscripts

$\bar{}$ = mean value
$n, n+1$ = time level
$\dot{}$ = time derivative

I. Introduction

IN SEPTEMBER 1991 an engine-powered remotely piloted ornithopter flew successfully for 2 min 46 s. This quarter-scale proof-of-concept model (Fig. 1) is described in Ref. 1. A second ornithopter model was built for the Canada Pavilion at Expo 1992 in Seville, Spain. This aircraft, appropriately named "Expothopter," was similar to the quarter-scale model in that it was completely flightworthy, but owing to the success of the quarter-scale model it was not necessary to fly the Expothopter.

Using the knowledge gained during the construction and testing of the quarter-scale model and Expothopter, a full-scale engine-powered human-carrying ornithopter (Fig. 2) was designed and built at the University of Toronto's Institute for Aerospace Studies. Details of the design, construction, and initial testing are described in Ref. 2. Results from the initial static-flapping (no forward speed) tests as well as some of the low-speed taxi tests are presented by Mehler.[3] The 1997 and 1998 taxi tests and the main bulk of the experimental data are discussed in detail by Fenton.[4]

An S1020 airfoil used in the quarter-scale model's wing was designed by Professor Michael Selig of the University of Illinois. This thick airfoil provides very high leading-edge suction efficiency as well as considerable structural depth. The full-scale ornithopter's wing also incorporates the S1020 airfoil. The inner portion of the wing uses this airfoil up to the "knuckle" (Fig. 4), and the outer tapered portion linearly transforms the S1020 to a Selig and Donovan SD8020 symmetrical airfoil at the tip. Figure 3 shows the airfoil shapes along the span of the full-scale ornithopter's wing. A rigid section, which is also known as the "SuperBox" (Fig. 4), is a closed structure made up of thin composite panels, internal ribs, a D-nose spar, and a rear shear web. Its function is to support the wing and transfer the loads to the outrigger struts. The outer rib of the SuperBox is referred to as the "SuperRib." The rest of the wing consists of 20 full-length ribs, made with a foam core and capped with basswood strips. The wing is covered with lightweight polyester fabric.

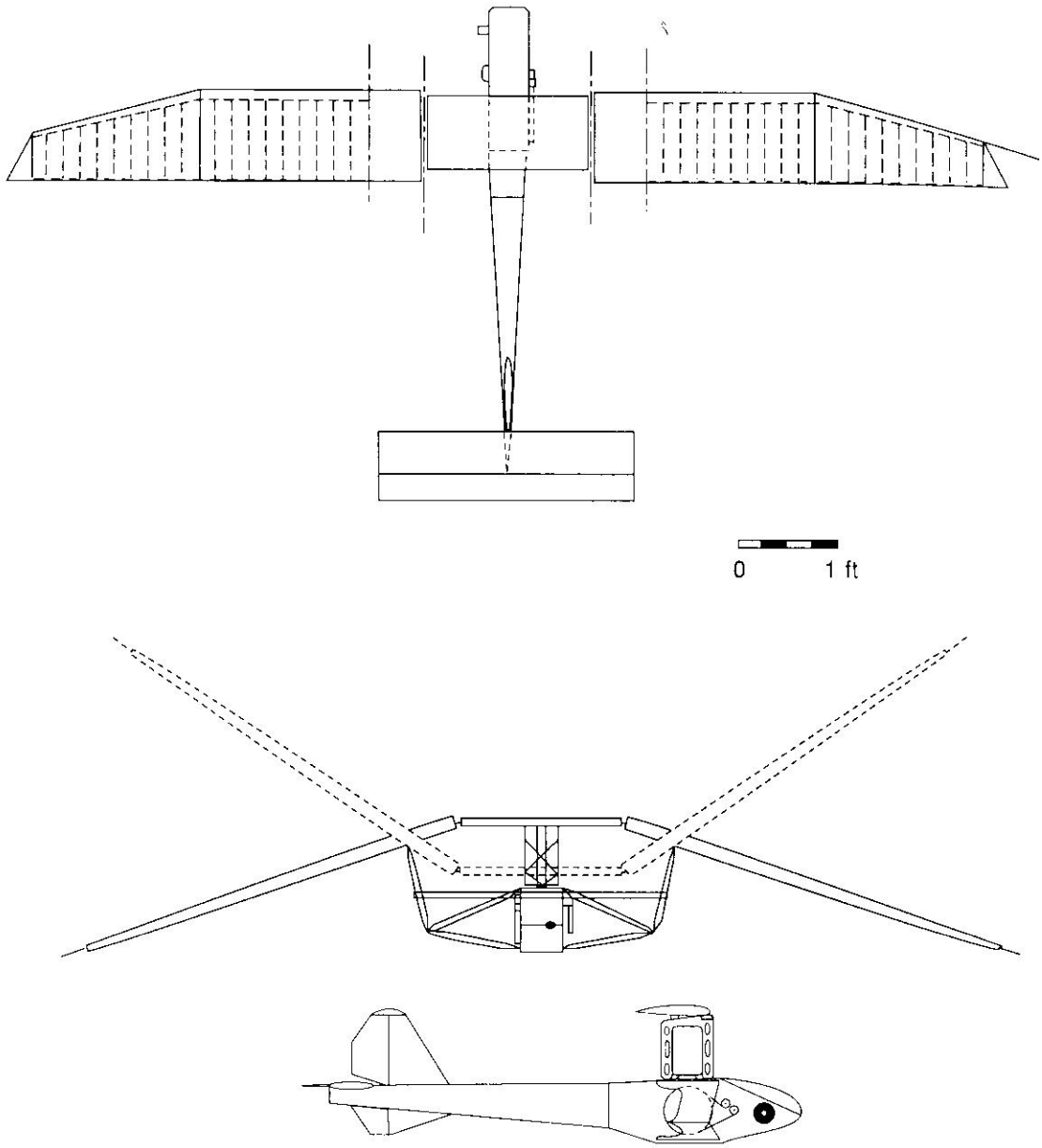

Fig. 1 Drawing of quarter-scale model ornithopter.

The center section is made up of composite panels, fore and aft shear webs, and nine internal ribs. The aerodynamic shape is created with a hollow blue-foam D-nose and nine half-length ribs. The cross section of the full-scale ornithopter wing spar (Fig. 5) is similar to that for the quarter-scale model. It is comprised of a carbon-fiber reinforced shear web for bending stiffness and strength, and a Kevlar® D-nose shell over a foam core for a structure of specified torsional compliance.[5]

A special feature of this wing's structure is that it is able to provide the required torsional compliance while at the same time incorporating the efficient and thick S1020 airfoil. Figure 6 shows how this is accomplished, where the closed torsion box normally formed by the thick airfoil is opened by splitting the trailing edge. This feature, patented as the "Shearflex Principle," allows a double-surface wing to have the high torsional compliance of two single-surface wings joined at the

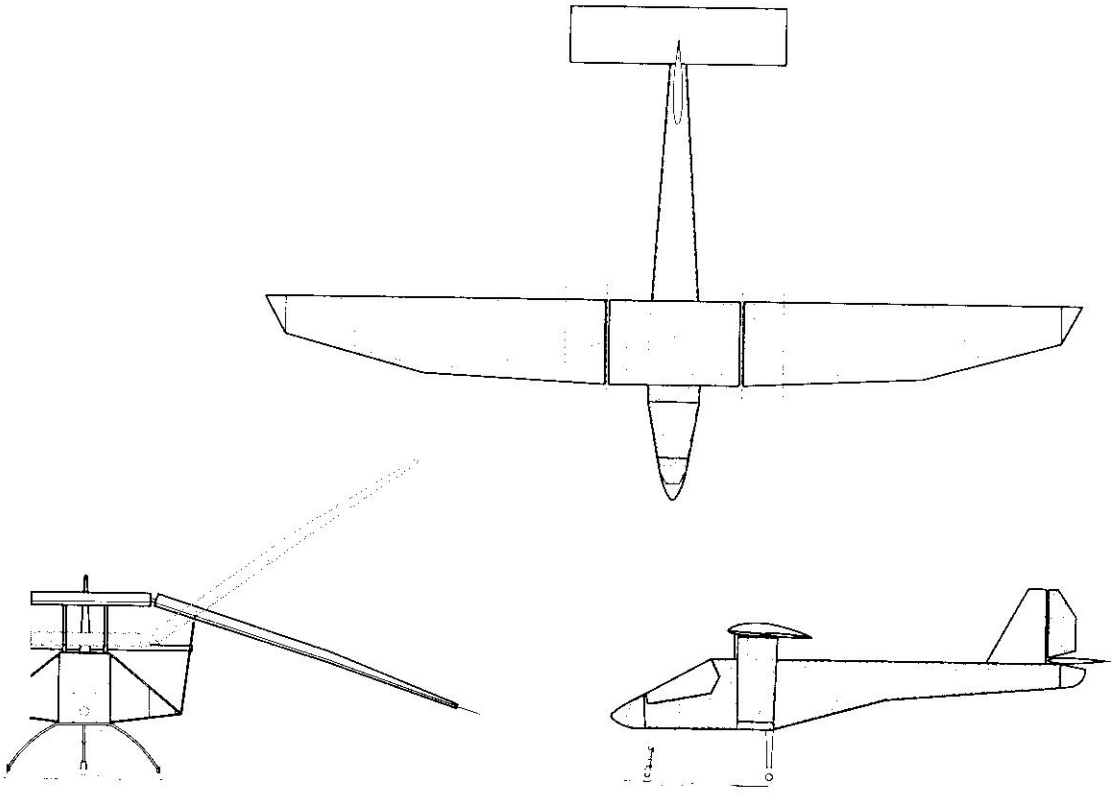

Fig. 2 Drawing of full-scale ornithopter.

leading edge. Therefore the ornithopter wing is able to twist freely even though its lightweight covering does not stretch. In fact, shearflexing would work well even if the skin were thick and relatively inflexible.

Analytical work done for the initial stages of the ornithopter project was based on a program called "Fullwing," which was developed to predict the performance of a flapping wing in steady flight.[6] Fullwing has gone through several revisions and it was most recently modified by the first author to improve its accuracy.

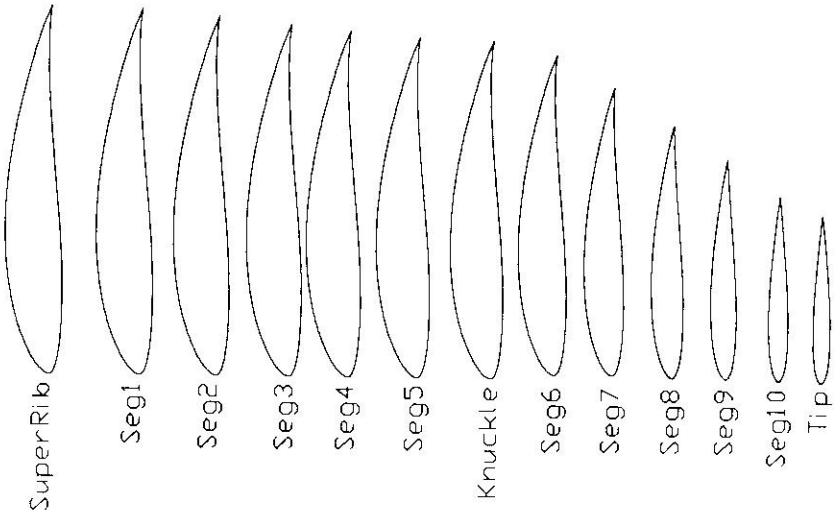

Fig. 3 Airfoils along the span.

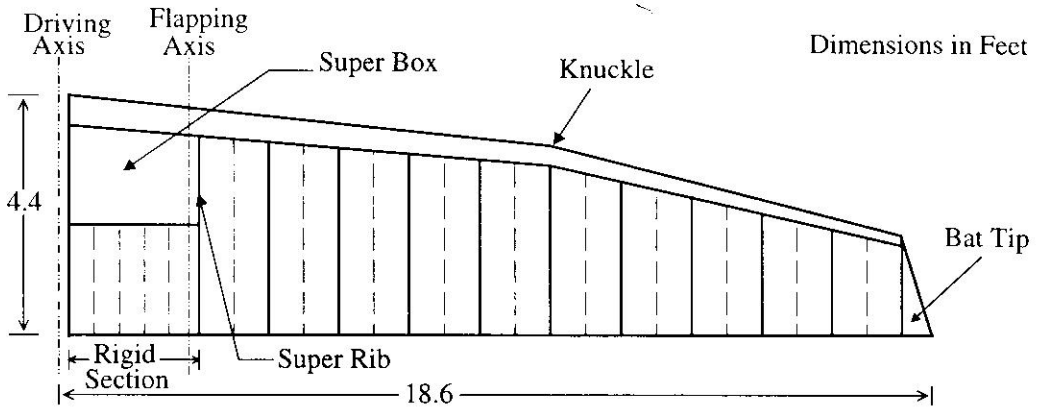

Fig. 4 Top view of ornithopter wing.

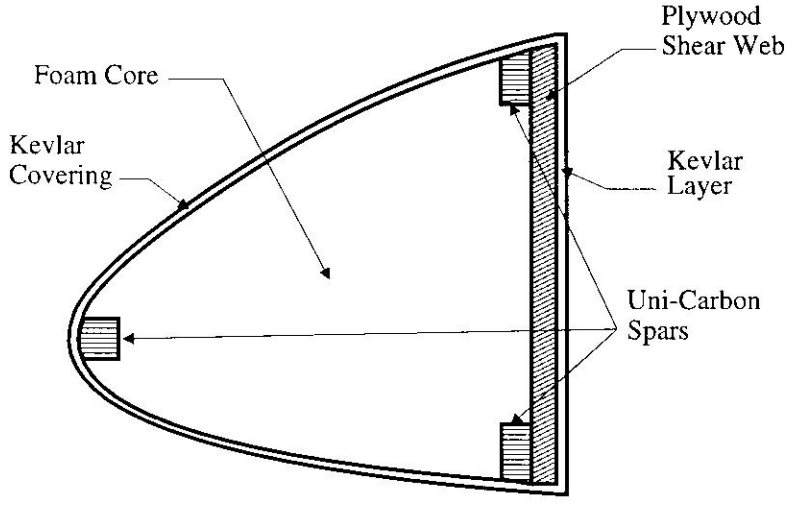

Fig. 5 Wing spar cross section.

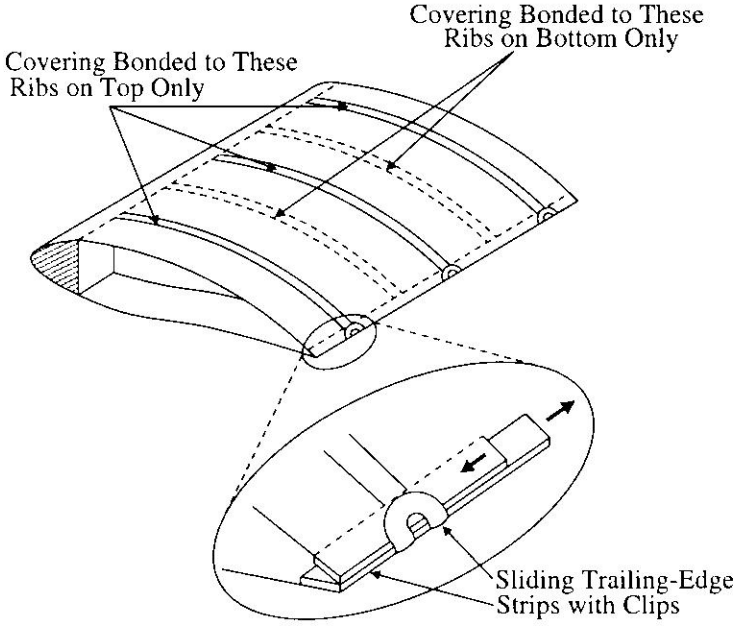

Fig. 6 Shearflexing principle.

The most significant assumption made in Fullwing is that of fully attached flow to linearize the equations. This gives inaccurate results as stalling dominates in the low forward-speed, high flapping-frequency regime, which became apparent during the static tests in 1996. It was noted that the phase angle between pitching and plunging was nowhere near the design value of approximately −90 deg. A "full-stall" formulation should give a more accurate representation of the problem. A second assumption is that the response has a simple harmonic motion. Although this is a reasonable description of the actual response, the presence of nonharmonic motion cannot be predicted. Also, its use of structural influence coefficients instead of a stiffness formulation has the disadvantage that for every new geometry the coefficients have to be rederived. An algorithm that uses transformation matrices can handle various geometric configurations more easily.

II. Structural Analysis

This section presents the linear ordinary differential equations governing the flapping motion of a wing and describes the matrices and vectors associated with them. The two principal modes of motion for a flapping wing are *bending* and *torsion*. A finite element discretization breaks the wing into spar elements with bending and torsional degrees of freedom and fabric and rib elements that have torsional degrees of freedom only (Fig. 7). For bending, the computational domain is divided into a set of elements, with each having two nodes (Fig. 8). A single element is then isolated and the Galerkin method[7] is applied, using a set of Hermite cubic interpolation functions, to derive the finite element formulation of the problem.

For torsion, the domain is also divided into a set of elements, with each element having two nodes as shown in Fig. 9. The Galerkin method is applied using a set of linear interpolation functions.

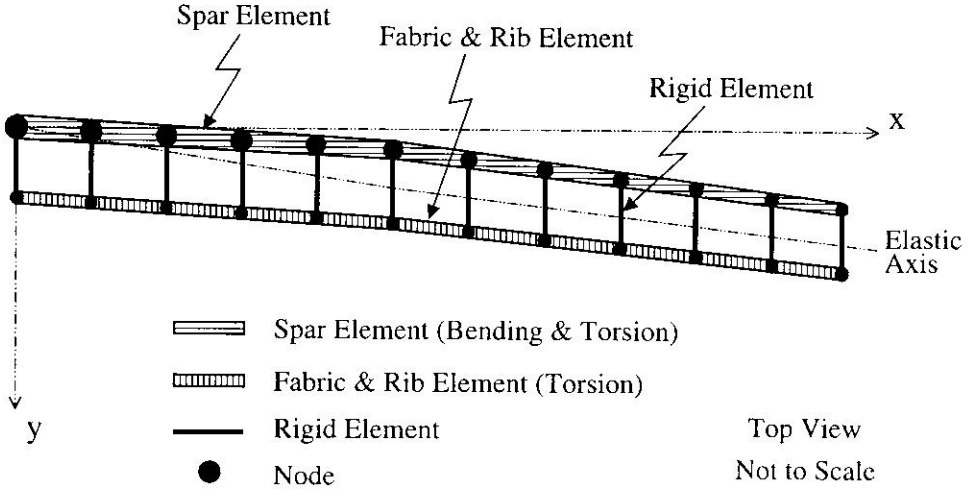

Fig. 7 Finite element discretization of ornithopter wing.

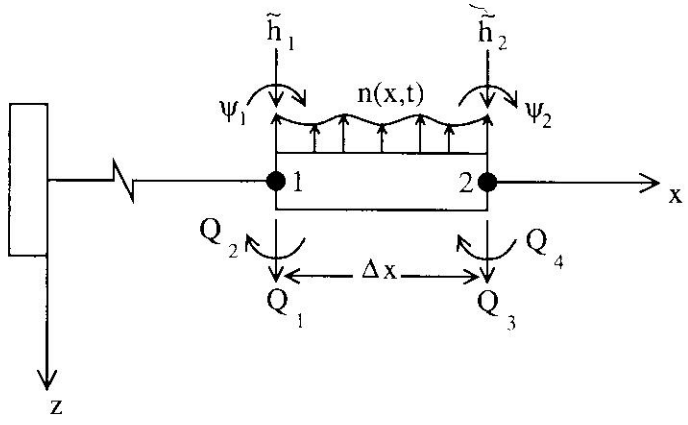

Fig. 8 Bending element.

The system dynamic equilibrium equations, including damping and neglecting external reactions, which are accounted for by boundary conditions, are

$$[\mathbf{K}]\{\mathbf{y}\} + [\mathbf{D}]\{\dot{\mathbf{y}}\} + [\mathbf{M}]\{\ddot{\mathbf{y}}\} = \{\mathbf{F}\} \tag{1}$$

The stiffness matrix for an element having both bending and torsional degrees of freedom is given by

$$[\mathbf{K}] = \begin{bmatrix} \frac{12EI}{\Delta x^3} & 0 & \frac{-6EI}{\Delta x^2} & \frac{-12EI}{\Delta x^3} & 0 & \frac{-6EI}{\Delta x^2} \\ 0 & \frac{GJ}{\Delta x} & 0 & 0 & \frac{-GJ}{\Delta x} & 0 \\ \frac{-6EI}{\Delta x^2} & 0 & \frac{4EI}{\Delta x} & \frac{6EI}{\Delta x^2} & 0 & \frac{2EI}{\Delta x} \\ \frac{-12EI}{\Delta x^3} & 0 & \frac{6EI}{\Delta x^2} & \frac{12EI}{\Delta x^3} & 0 & \frac{6EI}{\Delta x^2} \\ 0 & \frac{-GJ}{\Delta x} & 0 & 0 & \frac{GJ}{\Delta x} & 0 \\ \frac{-6EI}{\Delta x^2} & 0 & \frac{2EI}{\Delta x} & \frac{6EI}{\Delta x^2} & 0 & \frac{4EI}{\Delta x} \end{bmatrix} \tag{2}$$

where EI is the bending stiffness parameter, GJ is the corresponding torsional stiffness parameter for an element, and Δx is the length of a particular element. The overall consistent mass matrix for an element with total mass per unit length $\overline{m}$ is

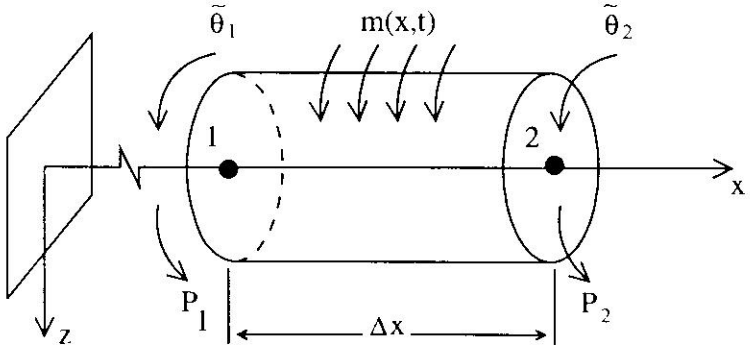

Fig. 9 Torsional element.

given by

$$[\mathbf{M}] = \overline{m}\Delta x \begin{bmatrix} \frac{156}{420} & 0 & \frac{-22\Delta x}{420} & \frac{54}{420} & 0 & \frac{13\Delta x}{420} \\ 0 & \frac{J}{3A} & 0 & 0 & \frac{J}{6A} & 0 \\ \frac{-22\Delta x}{420} & 0 & \frac{4\Delta x^2}{420} & \frac{-13\Delta x}{420} & 0 & \frac{-3\Delta x^2}{420} \\ \frac{54}{420} & 0 & \frac{-13\Delta x}{420} & \frac{156}{420} & 0 & \frac{22\Delta x}{420} \\ 0 & \frac{J}{6A} & 0 & 0 & \frac{J}{3A} & 0 \\ \frac{13\Delta x}{420} & 0 & \frac{-3\Delta x^2}{420} & \frac{22\Delta x}{420} & 0 & \frac{4\Delta x^2}{420} \end{bmatrix} \tag{3}$$

Assuming that the normal force and moment are constant over an element [i.e., $n(x, t) = n(t)$ and $m(x, t) = m(t)$] the force vector and the vector of independent variables are given by

$$\{\mathbf{F}\} = \begin{Bmatrix} -\frac{N(t)}{2} \\ \frac{M(t)}{2} \\ \frac{N(t)\Delta x}{12} \\ -\frac{N(t)}{2} \\ \frac{M(t)}{2} \\ -\frac{N(t)\Delta x}{12} \end{Bmatrix}, \qquad \{\mathbf{y}\} = \begin{Bmatrix} \tilde{h}_1 \\ \tilde{\theta}_1 \\ \psi_1 \\ \tilde{h}_2 \\ \tilde{\theta}_2 \\ \psi_2 \end{Bmatrix} \tag{4}$$

where $N(t) = n(t) \times \Delta x$ and $M(t) = m(t) \times \Delta x$. The aerodynamic forces and moments associated with a flapping wing in steady flight are nonlinear functions of the twisting and plunging deflections of the wing and their first and second derivatives. Equation (1) is a second-order nonlinear equation that is solved by using a Taylor series expansion to approximate the nonlinear components of the force vector. Several time-marching methods were considered and the nonlinear Newmark method was chosen because of its stability and ease of use. The nonlinear Newmark method is described in detail in Ref. 8. In the present study, since a temporal approximation has been used to obtain a set of linear second-order equations, an iteration must be performed at each time step to ensure that the equilibrium equations are satisfied. This iteration procedure is outlined by Owen.[9] The performance of the Newmark algorithm has been studied extensively and it is known to be unconditionally stable.[10]

III. Aerodynamic and Inertial Forces and Moments

The unsteady aerodynamic model for the study of a flapping wing is based on a modified strip theory approach. Vortex wake effects are accounted for as well as partial leading-edge suction and poststall behavior along with sectional mean angle of attack, camber, and friction drag. This model is then used for the calculation of average lift and thrust, power required, and propulsive efficiency of a flapping wing in equilibrium flight. A detailed treatment of this is given in Refs. 11 and 12.

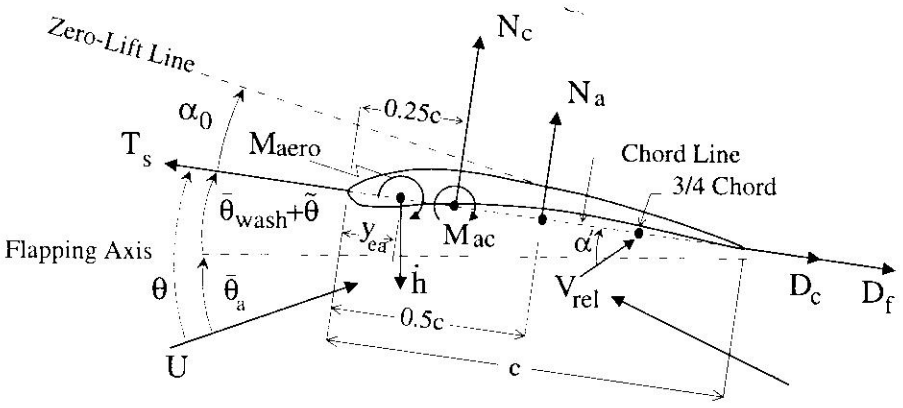

Fig. 10 Wing section aerodynamic forces and motion variables.

The starting point for the aerodynamic analysis is to determine the normal force N and moment M in Eq. (4) acting on a wing segment. For any element, M and N consist of aerodynamic and inertial terms:

$$N = N_{\text{aero}} + N_{\text{inertia}} \tag{5}$$

$$M = M_{\text{aero}} + M_{\text{inertia}} + M_{\text{damp}} \tag{6}$$

A. Aerodynamic Forces and Moments

The aerodynamic forces and moments are introduced in this section and the damping moment is treated separately in the next section along with the spar's structural damping. Figure 10 shows the aerodynamic forces on a representative segment (element) of the wing. Aerodynamic loads depend on whether the flow over a segment is attached or stalled.

1. Attached Flow

In the attached-flow regime the aerodynamic normal force is given by

$$N_{\text{aero}} = N_c + N_a \tag{7}$$

where N_c is the circulatory normal force and N_a is the apparent-mass normal force. The circulatory normal force on the wing segment is given by

$$N_c = \tfrac{1}{2}\rho U V C_n c \Delta x \tag{8}$$

where U is freestream air speed, c is the chord length of a particular segment, and Δx is the segment's length. V is the flow velocity at the $\frac{1}{4}$-chord location. Using small-angle assumptions, the normal force coefficient is shown to be[11]

$$C_n = 2\pi(\alpha' + \alpha_0 + \bar{\theta}_a + \bar{\theta}_{\text{wash}}) \tag{9}$$

where α_0 is the zero-lift angle, $\bar{\theta}_a$ is the flapping axis angle of attack, and $\bar{\theta}_{\text{wash}}$ is the built-in pretwist of the wing. α' is the flow's relative angle of attack at the $\frac{3}{4}$-chord point and is given by[11]

$$\alpha' = \frac{AR}{2+AR}\left[F'(k)\,\alpha + \frac{c}{2U}\frac{G'(k)}{k}\,\dot{\alpha}\right] - \frac{2[\alpha_0 + \bar{\theta}_a + \bar{\theta}_{\text{wash}}]}{2+AR} \tag{10}$$

Equation (10) is predicated on simple harmonic motion for α. In this case the motion can be periodic but not necessarily simple harmonic. Therefore, the use of this equation is considered to be an approximation to the unsteady shed wake effects. Each chordwise strip on the wing is assumed to act as if it were part of an elliptical planform wing executing simple harmonic whole-wing motion identical to that of the strip's. AR is the wing's aspect ratio and k is the reduced frequency, which is given by

$$k = \frac{c\omega}{2U} \tag{11}$$

Using a simplified formulation of the modified Theodorsen function, which was originally presented by Jones,[13] $F'(k)$ and $G'(k)$ are given by[11]

$$F'(k) = 1 - \frac{C_1 k^2}{k^2 + C_2^2}, \qquad G'(k) = -\frac{C_1 C_2 k}{k^2 + C_2^2}$$
$$C_1 = \frac{0.5\,AR}{2.32 + AR}, \qquad C_2 = 0.181 + \frac{0.772}{AR} \tag{12}$$

The equations for α and $\dot{\alpha}$ are (from Ref. 11)

$$\alpha = [\dot{h}\cos(\tilde{\theta} + \bar{\theta}_{\text{wash}}) + (0.75c - y_{ea})\dot{\tilde{\theta}}]/U + \tilde{\theta} \tag{13}$$

$$\dot{\alpha} = [(\ddot{h}_0 + \ddot{\tilde{h}})\cos(\tilde{\theta} + \bar{\theta}_{\text{wash}}) - \dot{h}\dot{\tilde{\theta}}\sin(\tilde{\theta} + \bar{\theta}_{\text{wash}}) + (0.75c - y_{ea})\ddot{\tilde{\theta}}]/U + \dot{\tilde{\theta}} \tag{14}$$

The Fullwing code uses a linear version of the above expression for $\dot{\alpha}$ by simply ignoring the second term in the numerator. The nonlinear Newmark code includes the complete expression.

It is appropriate at this point to introduce the total twist angle θ of a segment about its elastic axis, which is a combination of elastic and constant parts:

$$\theta = \tilde{\theta} + \bar{\theta}_a + \bar{\theta}_{\text{wash}} \tag{15}$$

Similarly, the total plunging displacement is a combination of an imposed motion h_0 and an elastic component $\tilde{h}$:

$$h = h_0 + \tilde{h} \tag{16}$$

The imposed motion for a given wing segment is defined as

$$h_0 = \Gamma_0 x \cos(\omega t) \tag{17}$$

where Γ_0 is the maximum flapping amplitude (which for the full-scale ornithopter is about 31 deg) and x is the distance from the center of a wing segment to the flapping axis. Returning to Eq. (8), we note that the flow velocity V must include the downwash as well as the wing's motion relative to the freestream velocity U. This is done by including α' along with the kinematic parameters:

$$V = \sqrt{[U\cos\theta - \dot{h}\sin(\tilde{\theta} + \bar{\theta}_{\text{wash}})]^2 + [U(\alpha' + \bar{\theta}_a + \bar{\theta}_{\text{wash}}) - (0.5c - y_{ea})\dot{\tilde{\theta}}]^2} \tag{18}$$

An additional normal-force contribution comes from the apparent-mass effect, which acts at the midchord location (Fig. 10) and is given by

$$N_a = \tfrac{1}{4}\,\rho\,\pi c^2\left(U\dot{\alpha} - \tfrac{1}{4}\,c\,\ddot{\bar{\theta}}\right)\Delta x \tag{19}$$

A section's circulation distribution generates forces in the chordwise direction as shown in Fig. (10). From DeLaurier,[14] the chordwise force due to camber is given by

$$D_c = -2\pi\alpha_0(\alpha' + \bar{\theta}_a + \bar{\theta}_{\text{wash}})\frac{\rho UV}{2}c\Delta x \tag{20}$$

The leading-edge suction force is obtained from Garrick[15] as

$$T_s = \eta_s 2\pi\left(\alpha' + \bar{\theta}_a + \bar{\theta}_{\text{wash}} - \frac{c\dot{\bar{\theta}}}{4U}\right)^2\frac{\rho UV}{2}c\Delta x \tag{21}$$

The only change to Garrick's formulation is the addition of the η_s term, which is referred to as the leading-edge suction efficiency factor and is determined experimentally. This efficiency factor is required since Garrick's formulation is based on ideal potential flow.

Viscous drag on the airfoil due to skin friction is found by using the skin-friction drag coefficient C_{df} for which an expression may be found in Hoerner.[16] Reference 11 presents this drag as

$$D_f = C_{df}\frac{\rho V_y^2}{2}c\Delta x \tag{22}$$

where V_y is the relative flow speed tangent to the section, which can be approximated by

$$V_y = U\cos\theta - \dot{h}\sin(\bar{\theta} + \bar{\theta}_{\text{wash}}) \tag{23}$$

Therefore the total chordwise force is

$$F_y = T_s - D_c - D_f \tag{24}$$

2. Stalled Flow

When the attached-flow range is exceeded, totally separated flow is assumed to abruptly occur, for which the contribution of chordwise forces is negligible:

$$T_s = D_c = D_f = 0 \tag{25}$$

and the normal force is given by

$$N = (N_c)_{\text{sep}} + (N_a)_{\text{sep}} \tag{26}$$

$(N_c)_{\text{sep}}$ acts at the midchord point and is due to crossflow drag and is assumed to be

$$(N_c)_{\text{sep}} = (C_d)_{cf}\frac{\rho\hat{V}V_n}{2}c\Delta x \tag{27}$$

where

$$\hat{V} = \sqrt{V_y^2 + V_n^2} \tag{28}$$

V_n is the midchord normal velocity component due to the wing's motion given by

$$V_n = \dot{h}\cos(\tilde{\theta} + \bar{\theta}_{\text{wash}}) + \tfrac{1}{2}c\,\dot{\theta} + U\sin\theta \tag{29}$$

and V_y is given by Eq. (23). It is evident from Eq. (28) that $\hat{V}$ is a nonlinear function of the independent variables $\tilde{\theta}$ and $\tilde{h}$. This shows that both the stalled and attached-flow aerodynamic formulations are indeed nonlinear.

Experiments conducted at the Institute for Aerospace Studies showed the value of the separated-flow apparent-mass normal force to be about half of that for attached flow. $(N_a)_{\text{sep}}$ is therefore assumed to be half of the value given by Eq. (19):

$$(N_a)_{\text{sep}} = \frac{N_a}{2} = \frac{1}{8}\,\rho\,\pi c^2\left(U\dot{\alpha} - \frac{1}{4}\,c\,\ddot{\tilde{\theta}}\right)\Delta x \tag{30}$$

3. Aerodynamic Moments

The attached-flow aerodynamic moment about the elastic axis is a function of the circulatory and apparent-mass normal forces and is given by

$$M_{\text{aero}} = M_{ac} - N_c(0.25c - y_{ea}) - N_a(0.5c - y_{ea}) - \frac{1}{16}\rho\pi c^3 U\,\Delta x\dot{\tilde{\theta}} - \frac{1}{128}\rho\pi c^4\,\Delta x\ddot{\tilde{\theta}} \tag{31}$$

N_c and N_a are given by Eqs. (8) and (19) respectively. The fourth and fifth terms in Eq. (31) account for the apparent camber and apparent inertia moments respectively.[11] The moment about the aerodynamic center is given by[17]

$$M_{ac} = C_{\text{mac}}\frac{\rho U V}{2}c^2\Delta x \tag{32}$$

The chordwise forces do not contribute to these moments as they essentially pass through the elastic axis of a wing segment.

The stalled aerodynamic moment is given by

$$(M_{\text{aero}})_{\text{sep}} = -[(N_c)_{\text{sep}} + (N_a)_{\text{sep}}](0.5c - y_{ea}) \tag{33}$$

where $(N_c)_{\text{sep}}$ and $(N_a)_{\text{sep}}$ are given by Eqs. (27) and (30) respectively. The moments about the aerodynamic center due to apparent camber and apparent inertia effects are negligible because these quantities are defined for attached flow only.

4. Stall Criterion

Prouty[18] has shown that a pitching airfoil can retain attached flow at angles greatly exceeding the airfoil's static stall angle. An advantage of a strip-theory model is that it allows for an approximation to the localized stall behavior. Prouty uses a dynamic stall-delay effect, represented by an angle $\Delta\alpha$, to account for the difference between the static and effective stall angles:

$$(\alpha_{\text{stall}})_{ef} - (\alpha_{\text{stall}})_{st} = \Delta\alpha = \xi\sqrt{\frac{c\,\dot{\alpha}}{2U}} \tag{34}$$

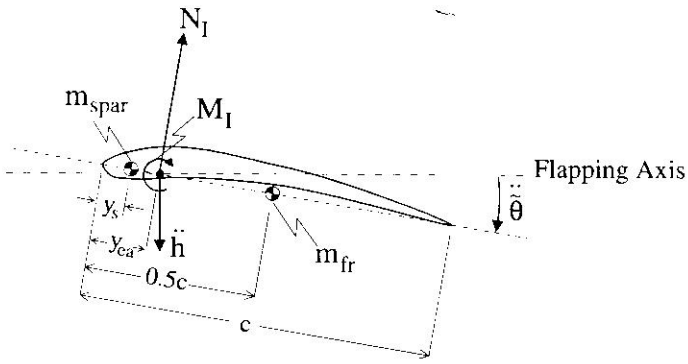

Fig. 11 Inertial loads and moments on a wing segment.

where ξ is found experimentally and depends on the local Mach number. In this case it was determined that $\Delta\alpha$ is given by[11]

$$\Delta\alpha = 0.51\left(\frac{\dot{\alpha}}{\dot{\alpha}_{\text{mag}}}\right)\sqrt{\frac{c\,\dot{\alpha}_{\text{mag}}}{2U}} \tag{35}$$

where $\dot{\alpha}_{\text{mag}} = \text{abs}(\dot{\alpha})$. The magnitude of $\dot{\alpha}$ is used to ensure that the term under the square root is positive and the term in the brackets ensures that the correct sign is used. Therefore, the criterion for attached flow over a wing segment is

$$(\alpha_{\text{stall}})_{\min} \leq \left[\alpha' + \bar{\theta}_a + \bar{\theta}_{\text{wash}} - \frac{3}{4}\left(\frac{c\dot{\bar{\theta}}}{U}\right)\right] \leq (\alpha_{\text{stall}})_{\max} \tag{36}$$

B. Inertial Forces and Moments

Figure 11 shows the inertial forces and moments acting on a wing segment. The Fullwing code treats the masses as inertial loads but the Newmark code breaks down the inertial loads into reactions that involve the elastic components and external forces that are a result of the imposed motion and gravity. The inertial reactions have already been considered by the consistent mass matrix formulation, and the external inertial normal force is given by[19]

$$N_{\text{inertia}} = (m_{\text{spar}} + m_{fr})(g_r - \ddot{h}_0) \tag{37}$$

Further, the external inertial moment is given by[19]

$$M_{\text{inertia}} = [(y_s - y_{ea})m_{\text{spar}} + (0.5c - y_{ea})m_{fr}](g_r - \ddot{h}_0) \tag{38}$$

where g_r is acceleration due to gravity.

C. Temporal Approximation for Nonlinear Terms

The most straightforward solution procedure is to use a nonlinear time-marching algorithm such as the fourth-order Runge–Kutta method. This would avoid the requirement of finding a temporal approximation to the nonlinear terms. An attempt was made to use this method to solve the dynamic equilibrium equations. However,

because of the presence of two distinct flow regimes and inherent instability, the solution would diverge after a few time steps.

It was noted in the previous section that the circulatory and apparent-mass normal forces are nonlinear functions of $\tilde{\theta}$, $\dot{\tilde{\theta}}$, $\ddot{\tilde{\theta}}$, $\dot{h}$, and $\ddot{h}$:

$$\begin{aligned} N_c &= f(\tilde{\theta}, \dot{\tilde{\theta}}, \ddot{\tilde{\theta}}, \dot{h}, \ddot{h}), \qquad N_a = f(\tilde{\theta}, \dot{\tilde{\theta}}, \ddot{\tilde{\theta}}, \dot{h}, \ddot{h}) \\ (N_c)_{\text{sep}} &= f(\tilde{\theta}, \dot{\tilde{\theta}}, \dot{h}), \qquad (N_a)_{\text{sep}} = f(\tilde{\theta}, \dot{\tilde{\theta}}, \ddot{\tilde{\theta}}, \dot{h}, \ddot{h}) \end{aligned} \tag{39}$$

The value of the circulatory normal force for attached flow at time $n+1$ is found by using a Taylor series approximation:

$$\begin{aligned} N_c^{n+1} = N_c^n &+ \frac{\partial N_c^n}{\partial \tilde{\theta}}[\tilde{\theta}^{n+1} - \tilde{\theta}^n] + \frac{\partial N_c^n}{\partial \dot{\tilde{\theta}}}[\dot{\tilde{\theta}}^{n+1} - \dot{\tilde{\theta}}^n] + \frac{\partial N_c^n}{\partial \ddot{\tilde{\theta}}}[\ddot{\tilde{\theta}}^{n+1} - \ddot{\tilde{\theta}}^n] \\ &+ \frac{\partial N_c^n}{\partial \dot{h}}[\dot{h}_0^{n+1} - \dot{h}_0^n] + \frac{\partial N_c^n}{\partial \dot{h}}[\dot{\tilde{h}}^{n+1} - \dot{\tilde{h}}^n] + \frac{\partial N_c^n}{\partial \ddot{h}}[\ddot{h}_0^{n+1} - \ddot{h}_0^n] \\ &+ \frac{\partial N_c^n}{\partial \ddot{h}}[\ddot{\tilde{h}}^{n+1} - \ddot{\tilde{h}}^n] \end{aligned} \tag{40}$$

Other normal-force components [Eqs. (19), (27), and (30)] and aerodynamic moments [Eqs. (31) and (33)] are also expanded in a similar way.

Terms involving the nth time step are moved to the right-hand side of the equilibrium equations [Eq. (1)] and terms involving the $(n+1)$'st time step are moved to the left-hand side of Eq. (1). Essentially, stiffness, mass, and damping matrices are augmented by terms that account for the nonlinearity of the forcing functions. Some authors (Refs. 10 and 20) refer to the augmenting matrices as tangent stiffness and tangent mass matrices.

D. Rigid and Center Sections

Aerodynamic forces and moments acting on the rigid and center sections of the wing are identical to those acting on the outer portion of the wing, and the same equations and the same criterion for stall can be used. The only difference is that the elastic variables are taken to be zero ($\tilde{\theta} = \tilde{h} = 0$). Furthermore, the forcing function for the rigid section is given by

$$(h_0)_{rs} = -\frac{(\Delta x)_{rs}}{2}\Gamma_0 \cos(\omega t) \tag{41}$$

where $(\Delta x)_{rs}$ is the width of the rigid section. Likewise, the center section forcing function is given by

$$(h_0)_{cs} = -(\Delta x)_{rs}\Gamma_0 \cos(\omega t) \tag{42}$$

E. Average Lift and Thrust

The total lift and thrust of a flapping wing at any given time is the sum of the contributions from the rigid, center, and flexible sections. The loads outlined in the previous section are normal N and tangential F_y to a given segment. Lift L and

thrust R for a particular segment of the flexible wing are calculated as follows:

$$R = F_y \cos(\theta) - N \sin(\theta), \qquad L = N \cos(\theta) + F_y \sin(\theta) \tag{43}$$

Lift and thrust produced by the rigid and center sections are calculated in a similar way. The average thrust and lift generated by the whole wing over N_l time intervals are

$$\begin{aligned} R_{\text{ave}} &= \frac{1}{N_l} \sum_{i=1}^{N_l} \left(2 \sum_{j=1}^{N_e} R_j + 2R_{rs} + R_{cs} \right)_i \\ L_{\text{ave}} &= \frac{1}{N_l} \sum_{i=1}^{N_l} \left(2 \sum_{j=1}^{N_e} L_j + 2L_{rs} + L_{cs} \right)_i \end{aligned} \tag{44}$$

where N_e is the total number of elements per wing.

F. Bending and Twisting Moments

The bending moments encountered at each wing segment are calculated by transforming the forces in the wing's frame of reference to the flapping-axis frame of reference. The flapping-axis angle of attack with respect to the freestream velocity can thus be accounted for. Hence, a new normal force F_{normal} must be defined:[5]

$$\begin{aligned} F_{\text{normal}} = {} & N \cos(\theta - \bar{\theta}_a) + (N_{\text{spar}} + N_{fr}) \cos(\bar{\theta}_a) \\ & + (T_s + D_f + D_c) \sin(\theta - \bar{\theta}_a) \end{aligned} \tag{45}$$

where normal forces acting on the spar and fabric and rib components are[19]

$$\begin{aligned} N_{\text{spar}} &= m_{\text{spar}}[\ddot{h} + (y_s - y_{ea})\ddot{\bar{\theta}} - g_r] \\ N_{fr} &= m_{fr}[\ddot{h} + (0.5c - y_{ea})\ddot{\bar{\theta}} - g_r] \end{aligned} \tag{46}$$

The bending moment at the flapping axis is thus calculated by adding up the contributions of all the segments on the flexible portion:

$$(M_{\text{bend}})_{sr} = \sum_{i=1}^{N_e} (F_{\text{normal}})_i \, x_i \tag{47}$$

where x_i is the distance of a given segment to the flapping axis. Similarly, the twisting moment is given by

$$(M_{\text{twist}})_{sr} = \sum_{i=1}^{N_e} (M_{ac})_i - (F_{\text{normal}})_i \, y_i \tag{48}$$

where y_i is the distance of the elastic axis for a given segment from a line perpendicular to the flapping axis and passing through the elastic axis at the flapping-axis location.

IV. Damping

Early in the development of the Newmark code it became apparent that a reliable damping model is required. Without a damping model and when using the Expothopter data file, the solution would diverge numerically. The reason was found to be that the undamped differential equations had positive eigenvalues. This showed that the initial theoretical model did not represent the actual system. However, this was in contradiction to what the Fullwing code predicted, as it did not have a damping model either. Furthermore, the Expothopter did perform reasonably well in wind tunnel tests conducted in Ottawa in 1995. At first it was believed that the cause was a set of stiff differential equations. However, examination of the system eigenvalues showed that the equations are not stiff. Finally, it was concluded that a damping model was required as that is the only component not accounted for by Fullwing. Furthermore, the shearflexing action of the wing creates damping forces along the trailing edge that must be accounted for.

The reason for Fullwing's predictions lies in the assumptions that were made when the code was developed, the most critical of which is that the output is assumed to be harmonic (sinusoidal) with a frequency equal to that of the forcing function. This basically guarantees that the output will not diverge. Therefore, when using a time-marching method, one must account for damping to obtain a stable solution.

Besides aerodynamic damping, there are two other forms of damping associated with a flapping wing:

1) *Fabric and rib damping*. This is a result of the frictional losses from the rubbing of the wing's fabric covering against the ribs caused by the shear flexing action. This action also contributes to damping as the trailing-edge strips rub against one another.

2) *Structural damping*. This is due to the viscoelastic losses in the spar. In homogeneous materials such as metals, this type of damping is relatively well understood and damping coefficients are known. In the case of the ornithopter wing, which is a nonhomogeneous material, experiments were conducted to determine the free-decay constant ζ for the overall wing.

A. Fabric and Rib Friction Damping

Experiments carried out in 1997 showed that the total damping moment is a combination of a constant value (M_{d0}) and a moment that is a function of the shear rate (M_{dsr}):

$$M_{\text{damp}} = M_{d0} + M_{dsr} \tag{49}$$

In terms of the friction force:

$$F_f = C_{f0} p A_{\text{con}} + C_f p A_{\text{con}} v_r \tag{50}$$

The first term on the right-hand side represents the shear-rate-independent friction force and the second term represents the shear-rate-dependent friction force. C_{f0} is the friction coefficient for the shear-rate-independent motion, and C_f is the friction, coefficient for the shear-rate-dependent motion; p is the contact pressure, and A_{con}, is the contact area between the surfaces. Also, v_r is the spanwise velocity of the upper surface relative to the lower surface of the wing.

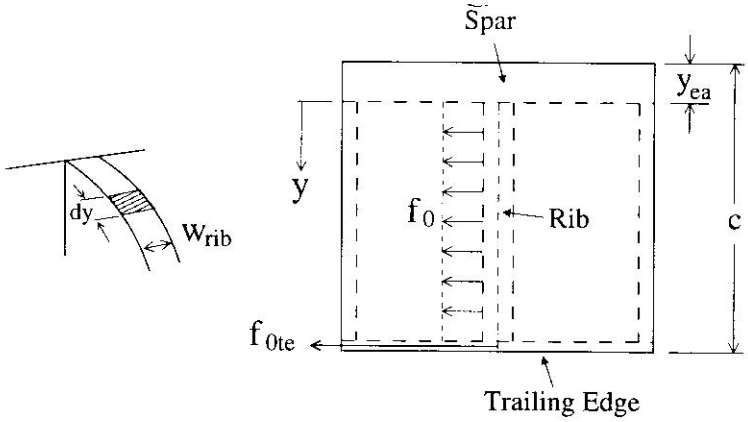

Fig. 12 Shear-rate-independent friction terms.

Considering the shear-rate-independent term and referring to Fig. 12, we can split the total friction force into a uniformly distributed fabric and rib force f_0 and a trailing-edge force f_{0te}:

$$f_0 = C_{f0} p w_{\text{rib}} \, dy \tag{51}$$

$$f_{0te} = C_{f0} p A_{te} \tag{52}$$

For a single wing segment the total shear-rate-independent damping moment is found by summing the moments about the elastic axis, which in Fig. 12 is shown to be the back of the spar. A_{te} is the contact area of the trailing-edge surface and w_{rib} is the width of a single rib. One thus has

$$M_{d0} = C_{f0} p A_{te}(c - y_{ea}) + C_{f0} p w_{\text{rib}} \int_0^{c-y_{ea}} dy \tag{53}$$

where c is the chord length of a particular wing section and y_{ea} is the distance from the leading edge to the elastic axis. M_{d0} is therefore given by

$$M_{d0} = C_{f0} p \, (c - y_{ea}) \left[A_{te} + \frac{w_{\text{rib}}}{2} (c - y_{ea}) \right] \text{sgn}(\dot{\tilde{\theta}}) \tag{54}$$

For the shear-rate-dependent damping moment, it is assumed that the friction force is related to velocity as shown by the second term on the right-hand side of Eq. (50). For each segment of the wing there is a twist/shear rate expressed as $\partial\theta/\partial x$, which is shown in Fig. 13. At this point we assume that the relative velocity of the upper surface to the lower surface v_r has a linear distribution, going from zero at the elastic axis to $v_r = v_{te}$ at the trailing edge. This gives rise to a friction force distribution as shown in Fig. 14. The two force components $f(y)$ and f_{te} are given by

$$f(y) = C_f p v_r(y) w_{\text{rib}} \, dy \tag{55}$$

$$f_{te} = C_f p v_{te} A_{te} \tag{56}$$

The shear-rate-dependent damping moment is thus given by

$$M_{\text{dsr}} = F_{te} \, (c - y_{ea}) + \int_0^{c-y_{ea}} f(y) y \, dA$$

$$= C_f p v_{te} \left[A_{te} \, (c - y_{ea}) + \frac{w_{\text{rib}}}{(c - y_{ea})} \int_0^{c-y_{ea}} y^2 \, dy \right] \tag{57}$$

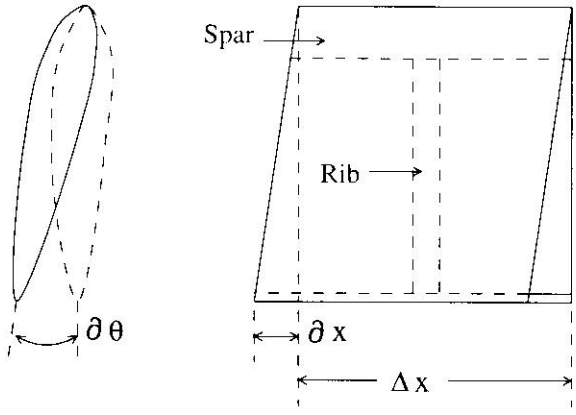

Fig. 13 Shear rate illustration.

Performing the integral on the right-hand side and simplifying gives

$$M_{\text{dsr}} = C_f p v_{te} (c - y_{ea}) \left[A_{te} + \frac{w_{\text{rib}}}{3} (c - y_{ea}) \right] \tag{58}$$

The velocity at the trailing edge can be written as

$$v_{te} = \frac{\partial x}{\partial t} = \frac{\partial x}{\partial \theta} \frac{\partial \theta}{\partial t} = \frac{\partial x}{\partial \theta} \dot{\theta} \tag{59}$$

so that M_{dsr} is finally given by

$$M_{\text{dsr}} = C_f p (c - y_{ea}) \left[A_{te} + \frac{w_{\text{rib}}}{3} (c - y_{ea}) \right] \left(\frac{\partial x}{\partial \theta} \right) \dot{\theta} \tag{60}$$

B. Structural Damping

Structural damping is primarily due to mechanisms such as hysteresis in the material and slip in connections. These mechanisms are not well understood and they are awkward to incorporate into the equilibrium equations. Therefore, the actual mechanism is usually approximated by viscous damping. Comparisons of theory and experiment show that this approach is sufficiently accurate in most cases.[20] With such approximate methods, experimental observations of the vibratory response of structures are used to assign a fraction of critical damping as a

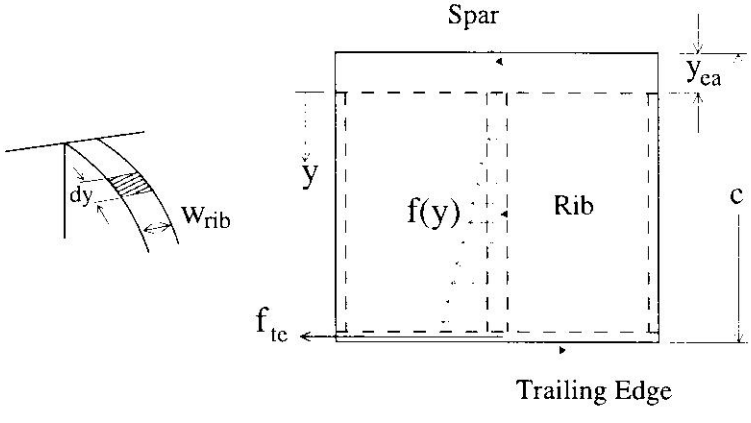

Fig. 14 Shear-rate-dependent friction forces.

function of frequency or, more commonly, a single decay constant ζ for the frequency range.

A popular damping scheme, called Rayleigh or proportional damping, is to form a damping matrix [**D**] as a linear combination of the stiffness and mass matrices, that is,

$$[\mathbf{D}] = a[\mathbf{M}] + b[\mathbf{K}] \tag{61}$$

where a and b are called the mass- and stiffness-proportional damping constants respectively. The damping matrix [Eq. (61)] is orthogonal because it permits modes to be uncoupled by eigenvectors associated with the undamped eigenvalues. The relationship among a, b, and decay constants ζ at a frequency ω is given by[20]

$$\zeta = \frac{a + \omega^2 b}{2\omega} \tag{62}$$

Damping constants a and b are determined by choosing two distinct decay constants (ζ_1 and ζ_2) at two different frequencies (ω_1 and ω_2) and solving simultaneous equations for a and b. Thus,

$$a = 2\omega_1\omega_2 \frac{\zeta_1\omega_2 - \zeta_2\omega_1}{\omega_2^2 - \omega_1^2}, \qquad b = 2\frac{\zeta_2\omega_2 - \zeta_1\omega_1}{\omega_2^2 - \omega_1^2} \tag{63}$$

As part of the work leading to the design of the full-scale ornithopter, several sample spars were constructed. One of these, known as Spar 6, was used to perform fatigue testing (Fig. 15). Spar 6's bending and torsional stiffness characteristics are identical to the actual wing spar's characteristics at the flapping-axis location.

In 1998, Spar 6 was used to determine its bending and torsional decay constants. Figure 16 shows Spar 6 in its bending configuration and Fig. 17 shows Spar 6 in its torsional configuration.

The testing procedure involved adding weights to the spar and striking it with a hammer while its vibratory response was measured using an accelerometer. The

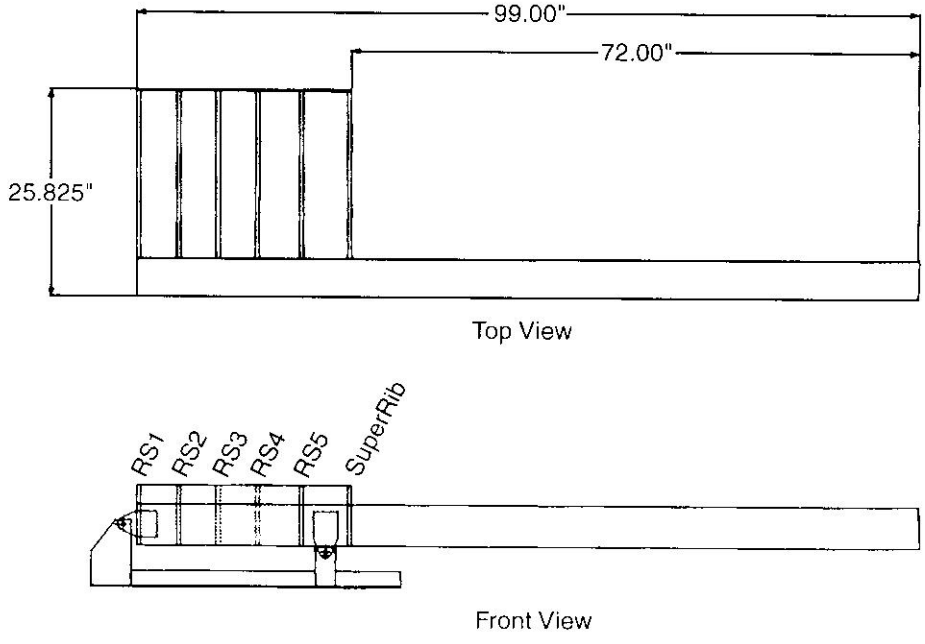

Fig. 15 Spar 6 schematic.

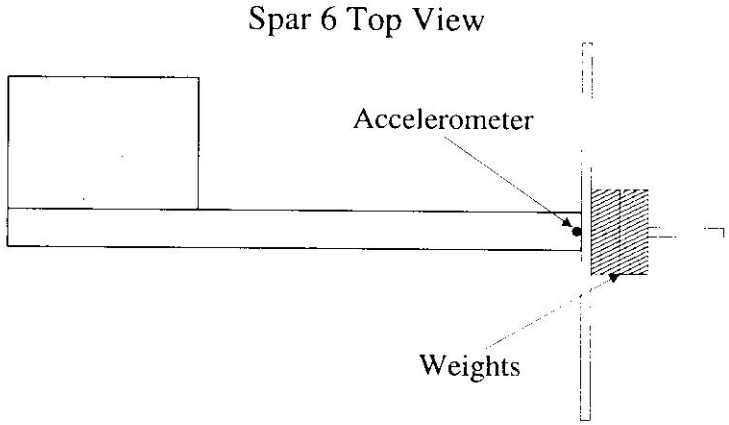

Fig. 16 Bending configuration.

weights were varied to produce a range of natural frequencies. Figure 18 shows the experimental results as well as a theoretical decay constant obtained using Rayleigh constants $a = 0.0136$ and $b = 0.0008$. It is evident from the graph that decay constants for bending and torsion are fairly constant over the range of frequencies tested. Basically, the Rayleigh model assumes a damping ratio that is within the limits prescribed by the two main damping modes. The Rayleigh model is also reasonable considering that the decay constants are on the order of 6×10^{-3}, or 0.6% of critical damping.

V. Results and Discussion

A large quantity of experimental data have been obtained during the design and testing of the two models as well as the full-scale ornithopter. The results of tests on the Expothopter are presented in a thesis by Fowler[5] and the bulk of experimental data for the full-scale ornithopter is contained in two M.S. theses by Mehler[3] and Fenton.[4] The objective of this section is to present a comparison between the nonlinear Newmark code and experimental results in all flight regimes, and to compare the Newmark and Fullwing codes at near-flight conditions.

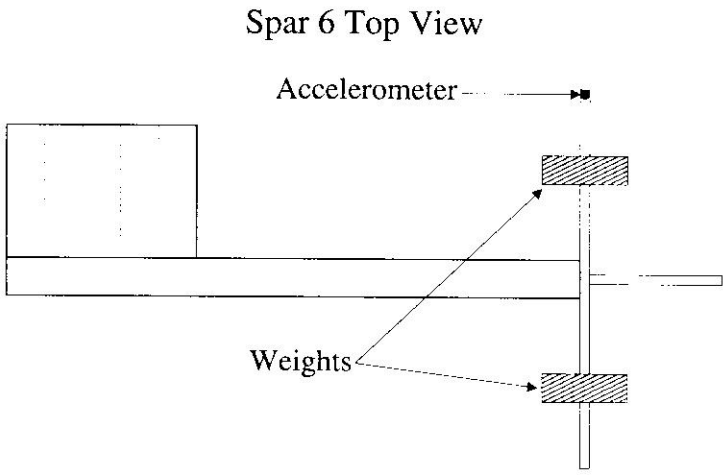

Fig. 17 Torsional configuration.

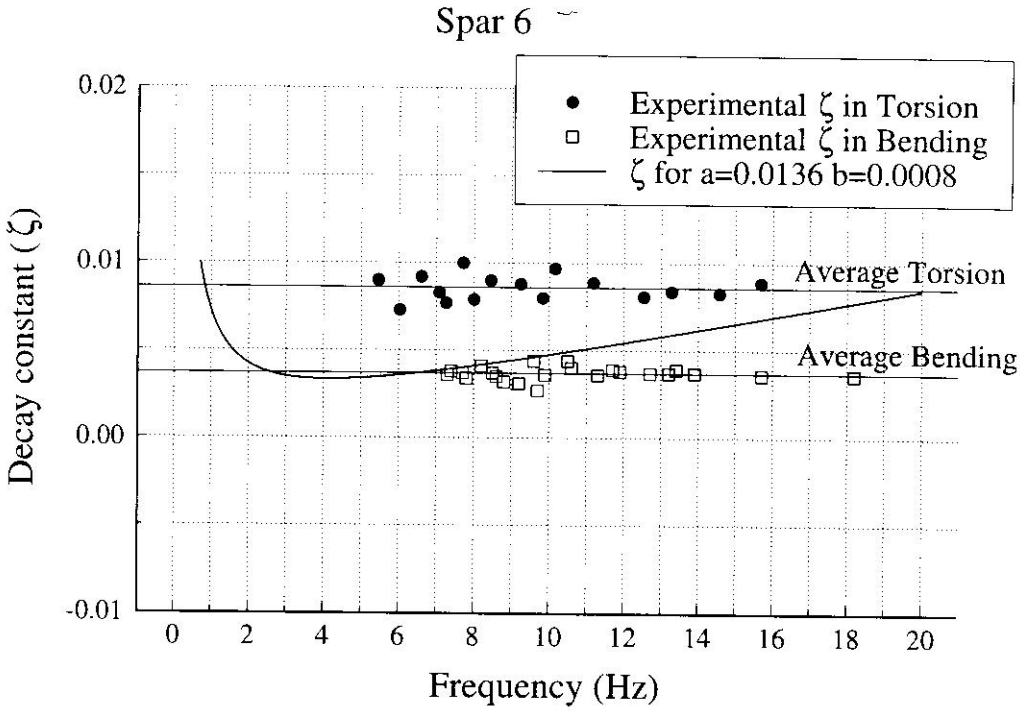

Fig. 18 Spar 6 decay constant variation.

A. Quarter-Scale Model Wing Tests

One of the wings of the quarter-scale model was attached to a flapping mechanism in the subsonic wind tunnel at the University of Toronto's Institute for Aerospace Studies.[12] The wing was also attached to scales that measured the generated average lift and thrust values at different flapping frequencies. Figures 19 and 20 show a comparison between theoretical results from Newmark and Fullwing codes as well as experimental data obtained during the tests. The discrepancy between theoretical and experimental lift is mainly due to the difference between

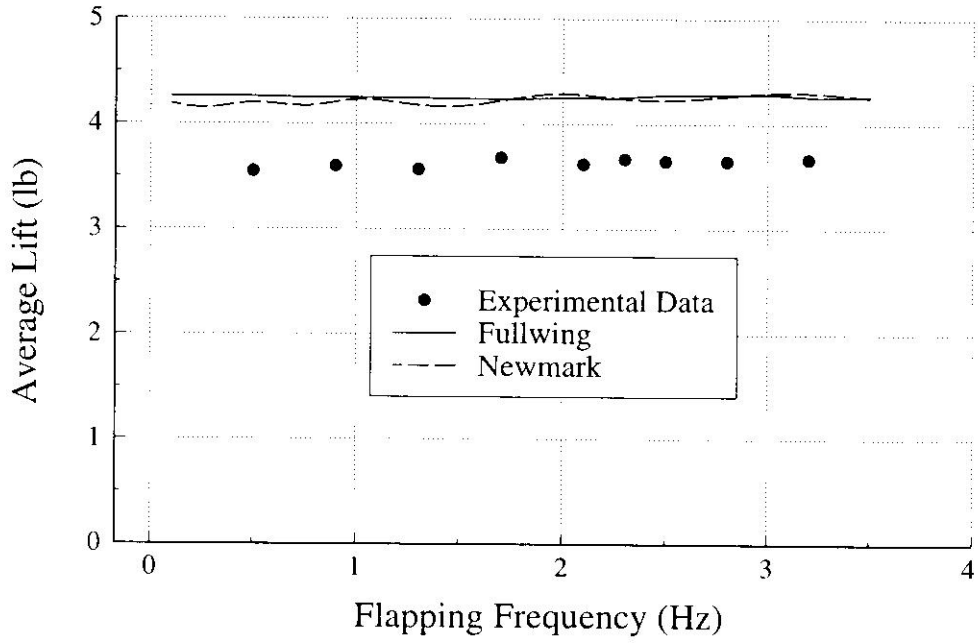

Fig. 19 Quarter-scale lift performance. U = 45 ft/s; $\tilde{\theta}_a$ = 6 deg.

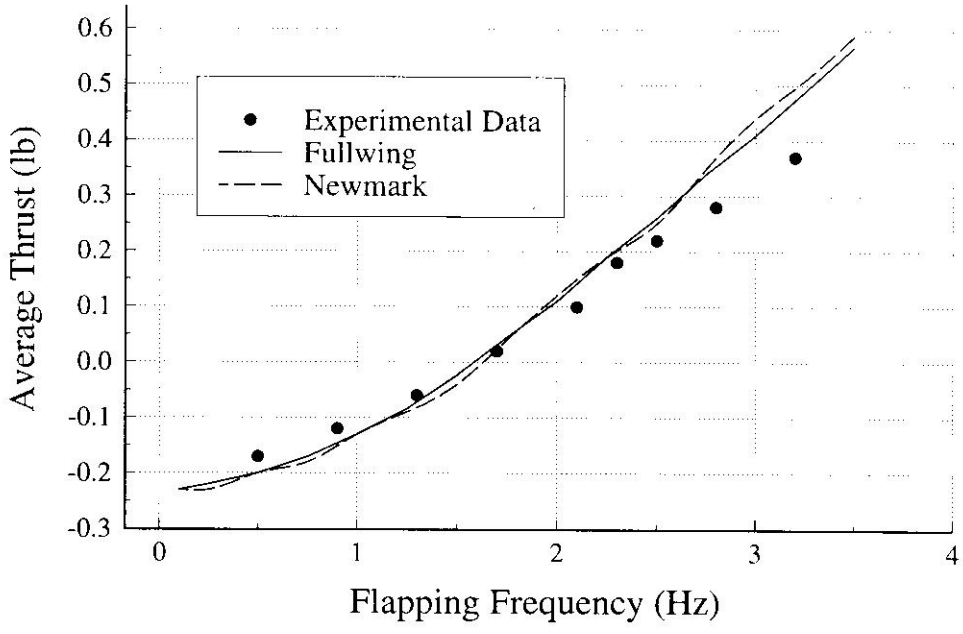

Fig. 20 Quarter-scale thrust performance. U = 45 ft/s; $\bar{\theta}_a$ = 6 deg.

the actual bending and torsional stiffness properties of the wing and the theoretical values used in the analysis.

B. 1996 Full-Scale Static-Flapping Tests

In 1996, a series of static-flapping tests were conducted. Strain gauges were attached to the wing at four locations as shown in Fig. 21 and twisting and bending moments were measured at different flapping frequencies. Figures 22 and 23 show a summary of maximum and minimum twisting and bending moment values for flapping frequencies from 0.4 to 1.1 Hz. Newmark's prediction is also shown. It should be recalled that the aerodynamic model is based on a strip theory. Such an approximation is limited, particularly in a fully-stalled flow regime.

Video footage of the wingtip motion was used to assess the twisting behavior of the wing and compare it to Newmark's predictions. Figures 24 and 25 show the wingtip twist at 0.91 and 0.97 Hz, respectively. It is evident from these figures that the nonlinear aerodynamic formulation is capable of predicting the wing's twisting behavior at conditions of zero forward speed.

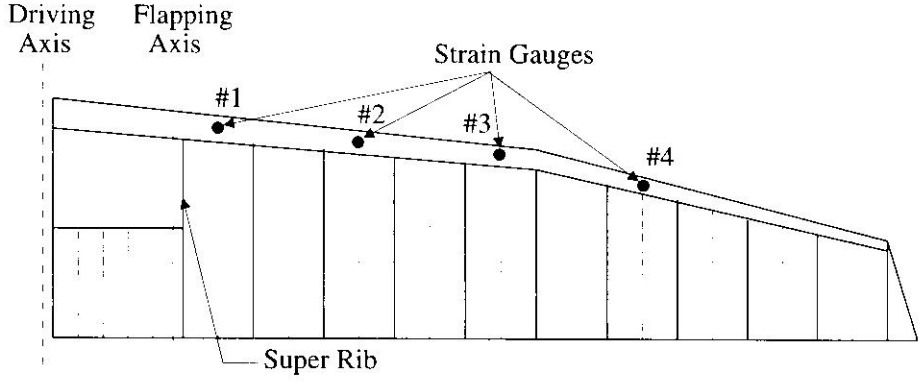

Fig. 21 Full-scale ornithopter strain gauge locations

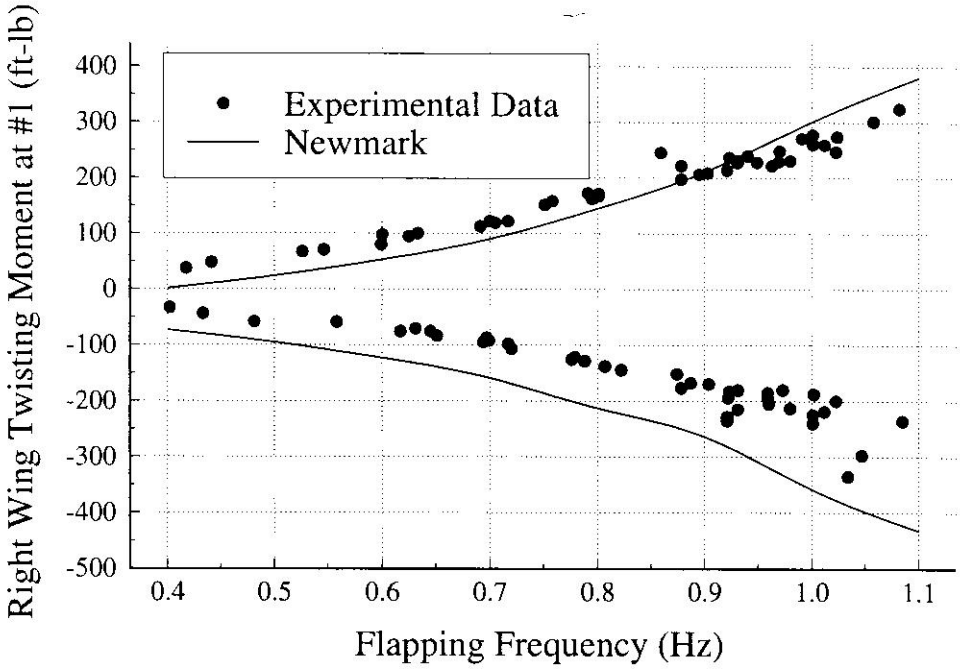

Fig. 22 Static twisting moment vs flapping frequency. U = 0.01 ft/s; $\bar{\theta}_a$ = 0 deg.

C. 1997 and 1998 Taxi Tests

In the summer of 1997 and 1998, extensive taxi trials were conducted at Downsview airport in Toronto. Figure 26 shows the ornithopter during a liftoff test in 1999. Unfortunately, all throughout 1997 and 1998 some strain gauges failed progressively and only a limited amount of data was collected. This is sufficient, however, to provide an opportunity for comparing the Newmark predictions with experimental data. Figures 27 and 28 show a summary of the maximum and

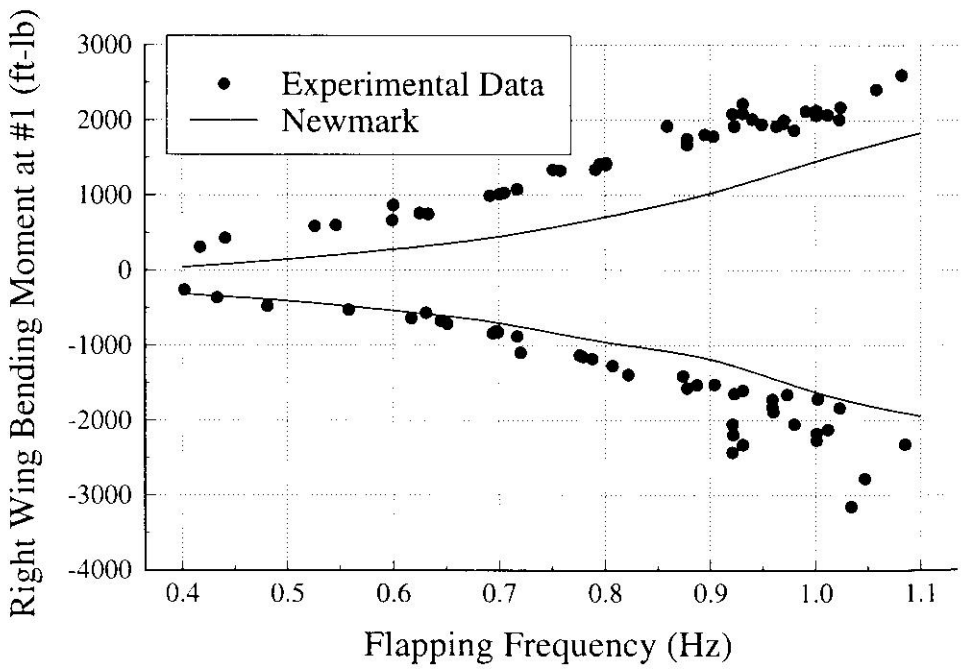

Fig. 23 Static bending moment vs flapping frequency. U = 0.01 ft/s; $\bar{\theta}_a$ = 0 deg.

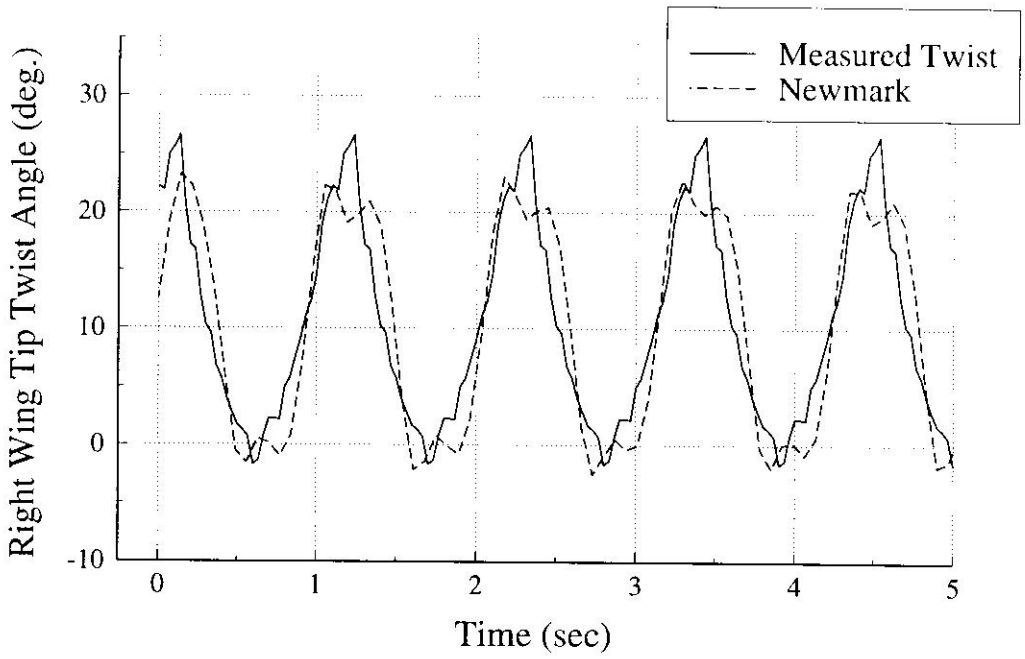

Fig. 24 Wing tip twist angle variation (ω = 0.91 Hz).

minimum twisting and bending moments during the 1997 and 1998 seasons. It should be noted that the reason for the limited amount of twisting-moment data is that all twisting-moment strain gauges had failed by the end of the 1997 season. Furthermore, the results presented here represent only portions of taxi tests where steady-state conditions were present. A steady-state condition in a taxi test would occur only when the throttle was maintained at a constant level and air speed was not rapidly changing. The reason for not connecting the data points on Figs. 27

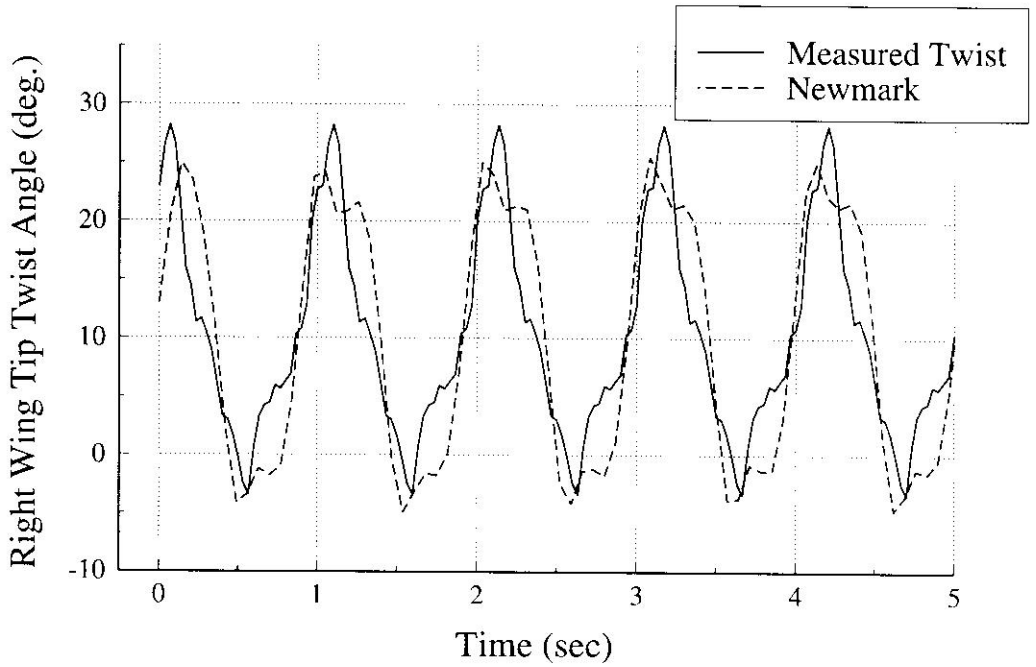

Fig. 25 Wing tip twist angle variation (ω = 0.97 Hz).

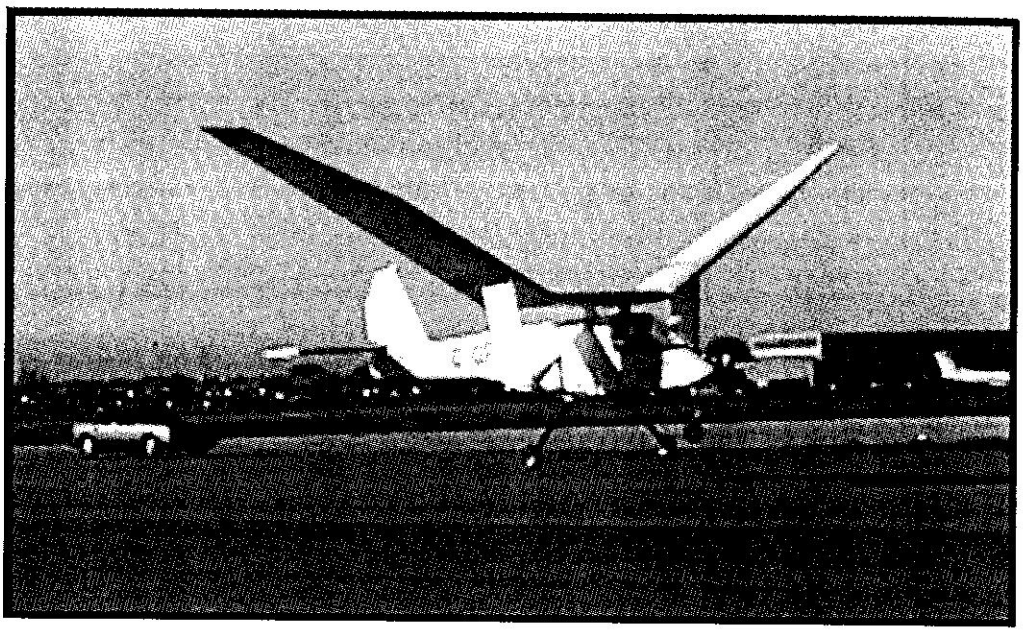

Fig. 26 Liftoff test in 1999.

and 28 is that each data point represents a run with different air speed U and angle of attack $\bar{\theta}_a$ values.

The strain gauges provided a significant quantity of instantaneous twisting- and bending-moment data as well. Figures 29 and 30 show the instantaneous twisting and bending moments during one of the runs in 1997. There is a maximum error of 20% associated with the twisting-moment data and about 15% for the bending-moment data.

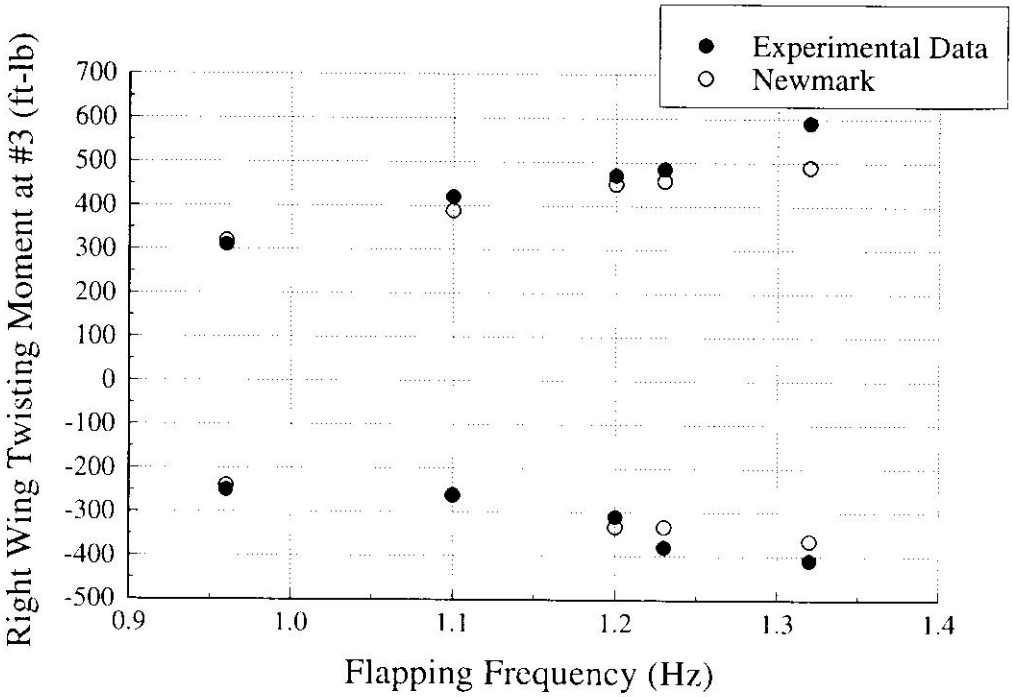

Fig. 27 Taxi test twisting moment vs flapping frequency.

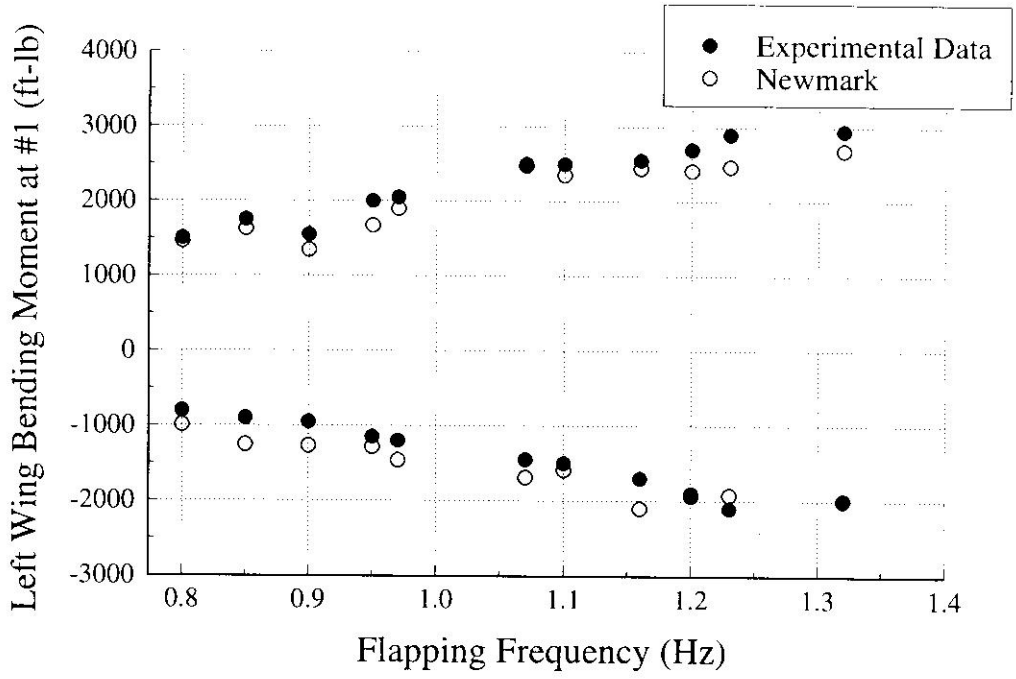

Fig. 28 Taxi test bending moment vs flapping frequency.

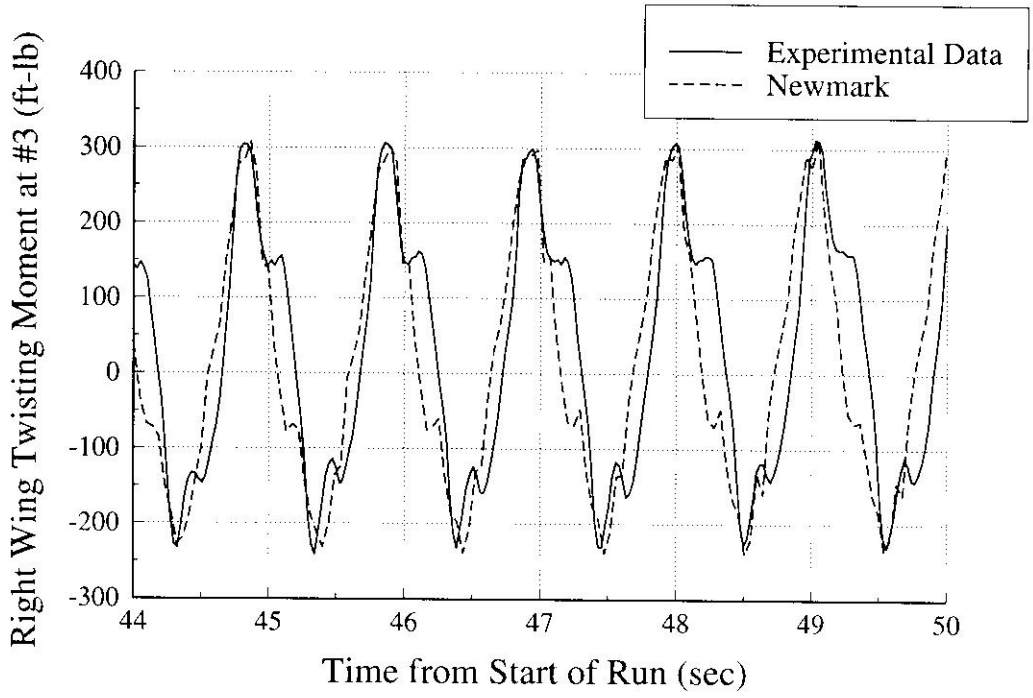

Fig. 29 Instantaneous twisting moment for run 1 on 15 September 1997. U = 44 ft/s; $\bar{\theta}_a$ = 3 deg; ω = 0.96 Hz.

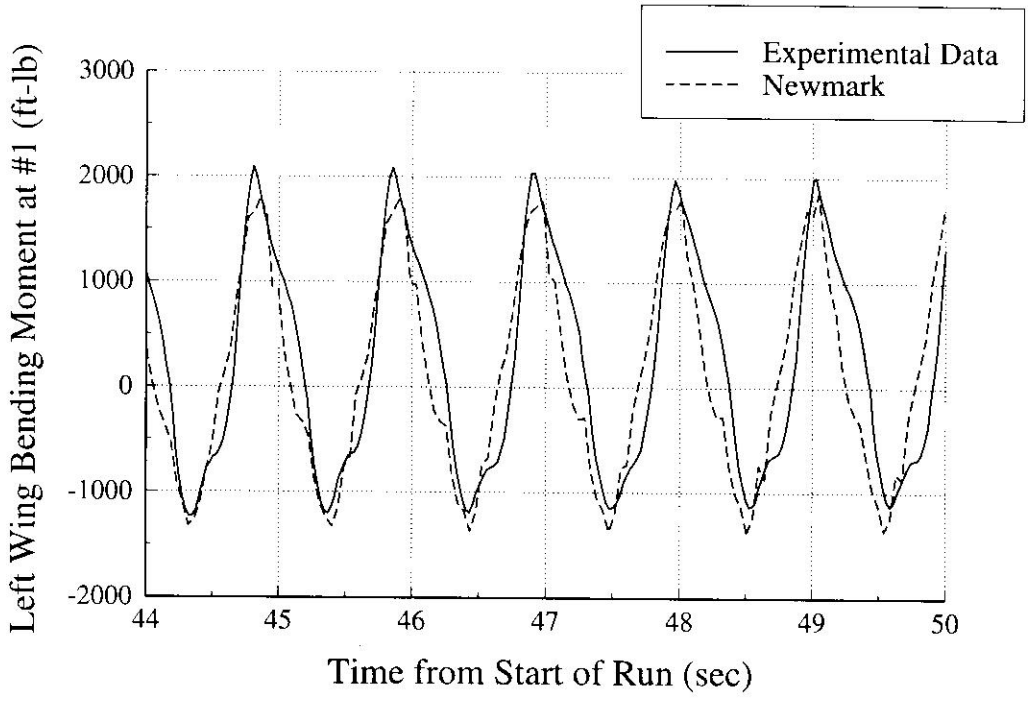

Fig. 30 Instantaneous bending moment for run 1 on 15 September 1997. U = 44 ft/s; $\bar{\theta}_a$ = 3 deg; ω = 0.96 Hz.

The Newmark code is very valuable for predicting lifting and thrusting performance of the wings, as shown in Figs. 31 and 32 for a flapping frequency of 1.2 Hz and an angle of attack $\bar{\theta}_a$ of zero. Although there is good agreement between Fullwing and Newmark average lift results, the static thrusting values are considerably different. As part of the 1996 static tests the value of average thrust at 1 Hz was measured to be about 25 lb. This, and the fact that in the 1997 and 1998 taxi trials the ornithopter was able to start its ground roll under its own power, shows that the Newmark thrust predictions are more accurate.

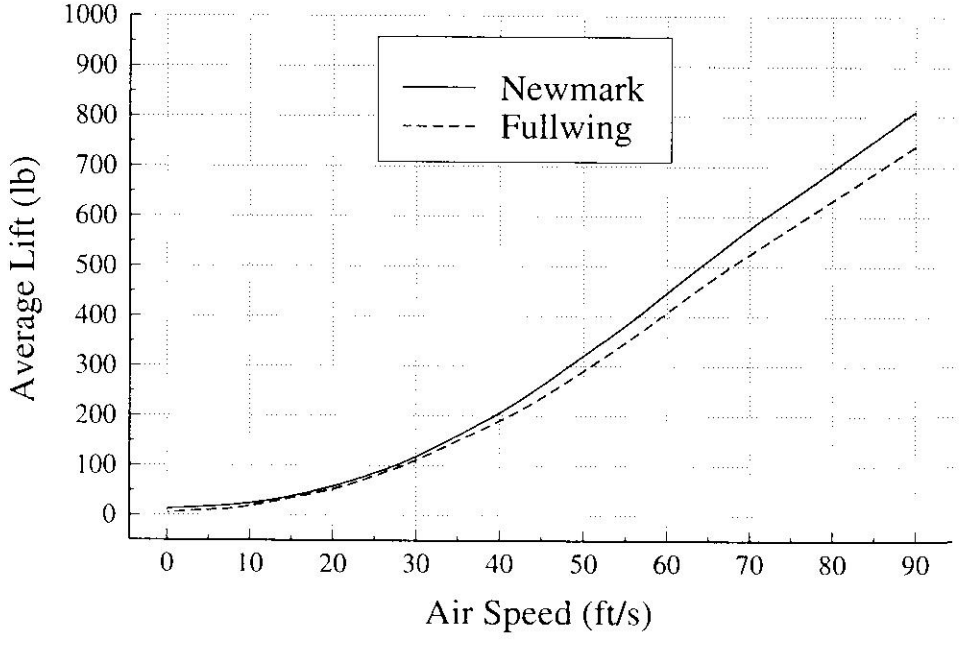

Fig. 31 Average lift vs air speed.

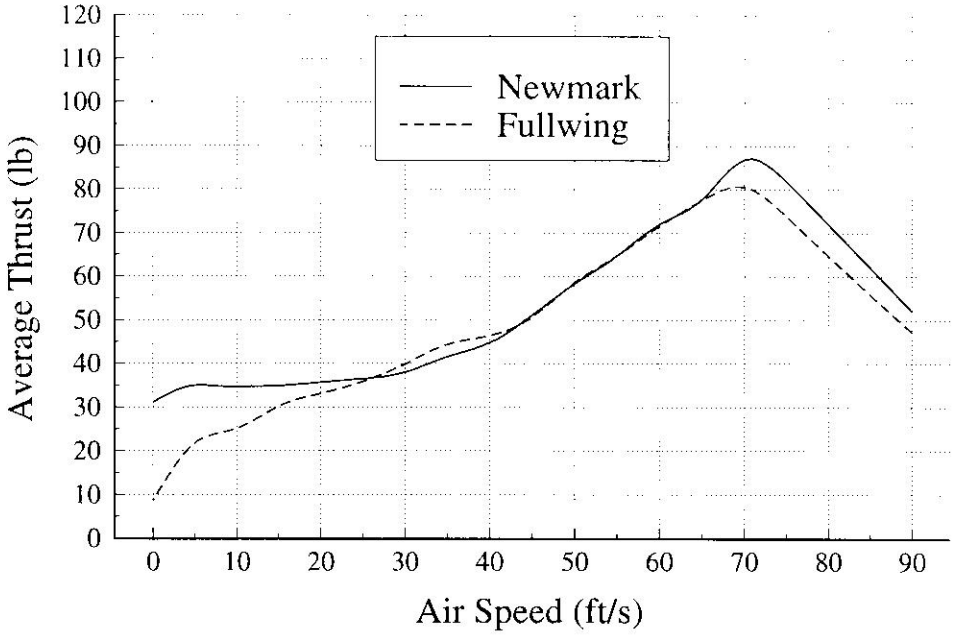

Fig. 32 Average thrust vs air speed.

VI. Conclusions

This chapter has presented an updated numerical method for predicting the performance of a flapping wing in steady flight. This is a design-oriented analysis using a nonlinear strip theory model for attached flow and poststall behavior. The finite element structural model that is used is both practical and versatile enough to handle different geometrical configurations with little or no modifications. A translational matrix formulation eliminates the need for cross members that would have otherwise been required to connect the spar and fabric and rib elements to one another. The Rayleigh damping model is a convenient way for modeling the damping characteristics of the spar, and experimental data were used to determine approximate values for bending and torsional decay constants associated with a sample spar. The Rayleigh model is also suitable because the spar's decay constant is about 0.6% of critical damping. The fabric and rib friction-damping model account for the energy loss caused by the shearflexing action of the wing. This damping model is necessary since shearflexing is a unique feature of the ornithopter's wing.

The Newmark predictions for maximum and minimum twisting moment during static flapping are quite accurate and much better than expected considering the relatively simple aerodynamic model used. There is a maximum error of about 25% associated with the maximum and minimum bending moments at the flapping-axis location for static flapping.

One of the issues raised during the 1996 static-flapping tests was the unexpected twisting behavior of the wings. This was particularly worrisome at the time because the phase angle between flapping and twisting was not close to the optimum value of approximately −90 deg. By properly modeling the fully stalled characteristics of the wing it became possible to predict the correct wing twisting behavior at near-static conditions. This basically shows that severe stalling at near-static conditions produces a twisting behavior that is far from optimum. This is possibly the most important contribution from the analysis.

There is better agreement between theory and experimental data for near-flight conditions. The maximum error for maximum and minimum bending and torsion

still functioning were more than two-years old and were beginning to suffer from adhesive deterioration.

This analysis has not only helped the research team at the Institute for Aerospace Studies better understand the aerodynamic characteristics of the ornithopter's wings, but it will also provide a valuable tool for future design of flapping wing aircraft.

References

[1]DeLaurier, J. D., and Harris, J. M., "A Study of Mechanical Flapping Wing Flight," *Aeronautical Journal*, Vol. 97, No. 968, Oct. 1993, pp. 277–286.

[2]DeLaurier, J. D., "The Development and Testing of a Full-Scale Piloted Ornithopter," *Canadian Aeronautics and Space Journal*, Vol. 45, No. 2, June 1999, pp. 72–82.

[3]Mehler, F. E., "The Structural Testing and Modification of a Full-Scale Ornithopter's Wing Spars," M.A.Sc. Thesis, Faculty of Applied Science and Engineering, University of Toronto, Downsview, ON, Canada, 1997.

[4]Fenton, B. A., "The Testing and Modification of a Full-Scale Ornithopter," M.A.Sc. Thesis, Faculty of Applied Science and Engineering, University of Toronto, Downsview, ON, Canada, 1999.

[5]Fowler, S. J., "The Design and Development of a Wing for a Full-Scale Piloted Engine-Powered Flapping Wing Aircraft (Ornithopter)," M.A.Sc. Thesis, Faculty of Applied Science and Engineering, University of Toronto, Downsview, ON, Canada, 1995.

[6]DeLaurier, J. D., "An Ornithopter Wing Design," *Canadian Aeronautics and Space Journal*, Vol. 40, No. 1, March 1994, pp. 10–18.

[7]Reddy, J. N., *An Introduction to the Finite Element Method*, McGraw-Hill, New York, 1984.

[8]Bathe, K. J., *Finite Element Procedures*, Prentice-Hall, Englewood Cliffs, NJ, 1996.

[9]Owen, D. R. J., "Implicit Finite Element Methods for the Dynamic Transient Analysis of Solids with Particular Reference to Non-Linear Situations," *Advanced Structural Dynamics*, Applied Science Publishers, London, 1978, pp. 123–152.

[10]Humar, J. L., *Dynamics of Structures*, Prentice-Hall, Englewood Cliffs, NJ, 1990.

[11]DeLaurier, J. D., "An Aerodynamic Model for Flapping Wing Flight," *Aeronautical Journal*, Vol. 97, April 1993, pp. 125–130.

[12]DeLaurier, J. D., "The Development of an Efficient Ornithopter Wing," *Aeronautical Journal*, Vol. 97, May 1993, pp. 153–162.

[13]Jones, R. T., "The Unsteady Lift of a Wing of Finite Aspect Ratio," NACA Rept. 681, 1940.

[14]DeLaurier, J. D., "Drag of Wings with Cambered Airfoils and Partial Leading Edge Suction," *Journal of Aircraft*, Vol. 20, Oct. 1983, pp. 882–886.

[15]Garrick, I. E., "Propulsion of a Flapping and Oscillating Aerofoil," NACA Rept. 567, 1936.

[16]Hoerner, S. F., *Fluid Dynamic Drag*, published by the author, Brick Town, NJ, 1965, pp. 2-1 to 2-16.

[17]DeLaurier, J. D., "Time Marching Solution for Elastic Flapping Wings," 1997 (unpublished personal notes).

[18]Prouty, R. W., *Airfoils for Rotor Blades, Helicopter Performance, Stability and Control*, PWS Engineering, Boston, 1986.

[19]Larijani, R. F., "Inertial Forces and Moments for a Second Order Non-Linear Formulation," 2000 (unpublished personal notes).

[20]Cook, R. D., Malkus, D. S., and Plesha, M. E., *Concepts and Applications of Finite Element Analysis*, Wiley, New York, 1996.